

# Picosecond Ultrasonics with Miniaturized Semiconductor Lasers

Michal Kobecki,<sup>1</sup> Giuseppe Tandoi,<sup>2</sup> Eugenio Di Gaetano,<sup>2</sup> Marc Sorel,<sup>2</sup> Alexey V. Scherbakov,<sup>1,3</sup> Thomas Czerniuk,<sup>1</sup> Christian Schneider,<sup>4</sup> Martin Kamp,<sup>4</sup> Sven Höfling,<sup>4</sup> Andrey V. Akimov,<sup>5,\*</sup> Manfred Bayer<sup>1,3</sup>

<sup>1</sup> *Experimentelle Physik 2, Technische Universität Dortmund, D-44221 Dortmund, Germany*

<sup>2</sup> *School of Engineering, University of Glasgow, Glasgow, G12 8QQ, United Kingdom*

<sup>3</sup> *Ioffe Institute, 194021 St. Petersburg, Russia*

<sup>4</sup> *Technische Physik, Universität Würzburg, 97074 Würzburg, Germany*

<sup>5</sup> *School of Physics and Astronomy, University of Nottingham, Nottingham NG7 2RD, United Kingdom*

**Abstract:** There is a great desire to extend ultrasonic techniques to the imaging and characterization of nanoobjects. This can be achieved by picosecond ultrasonics, where by using ultrafast lasers it is possible to generate and detect acoustic waves with frequencies up to terahertz and wavelengths down to nanometers. In our work we present a picosecond ultrasonics setup based on miniaturized mode-locked semiconductor lasers, whose performance allows us to obtain the necessary power, pulse duration and repetition rate. Using such a laser, we measure the ultrasonic echo signal with picosecond resolution in a 112 nm thick Al film deposited on a semiconductor substrate. We show that the obtained signal is as good as the signal obtained with a standard bulky mode-locked Ti-Sa laser. The experiments pave the way for designing integrated portable picosecond ultrasonic setups on the basis of miniaturized semiconductor lasers.

Keywords: Picosecond ultrasonics  
Semiconductor lasers  
Coherent Phonons

Corresponding author: \* [andrey.akimov@nottingham.ac.uk](mailto:andrey.akimov@nottingham.ac.uk)

## 1. Introduction

Picosecond ultrasonics (PU) is an advanced research field which aims to extend traditional acoustic techniques to the gigahertz (GHz) and terahertz (THz) frequency ranges [1,2]. It started in the late 1980ies with the development of ultrafast lasers and nowadays PU shows great potential for elastic nanoscopy [3] and ultrafast control of electronic and optical devices [4-6]. PU imaging with sub-nanometer depth resolution is used to study nanostructures [7,8] including biological objects [9-11], chemical reactions [12], adhesion of nanolayers [13,14] and profile inhomogeneity [15].

The main element of a PU setup is a pico- or femtosecond laser which output is split in two beams used for pumping and probing the system of interest. In most of PU experiments the pump beam is focused onto a thin metal film which acts as an thermoelastic transducer. After being hit by the pump pulse, the film expands in a time of  $\sim 1$  ps and, as a consequence, a coherent elastic wave packet with frequencies up to several hundreds of GHz is injected into the specimen or device. The critical parameters for PU is the energy density  $J$  in the focus spot of the laser pump pulse, the pulse duration  $\Delta t$ , which limits the temporal resolution and correspondingly the maximum frequency in the ultrasonic wave packet, and the laser repetition rate  $f$ , which determines the accumulation time. The values for  $J$ ,  $\Delta t$  and  $f$  that can reliably be reached, cover a wide range ( $J=10^{-6}$ - $10^{-2}$  J/cm<sup>2</sup>,  $\Delta t \leq 1$  ps and  $f=10$ - $10^9$  Hz) using different experimental schemes and can easily be achieved using commercial femtosecond lasers. However, all PU setups are mounted on optical tables and use bulky, not portable lasers which so far has limited the application potential of PU in geology, biology and medicine.

Therefore, it is very attractive to develop a portable PU setup with the elements integrated on a single chip which would facilitate its flexible application to an object and perform PU in situ during a short exposure time. The main element of such a prospective device is the ultrafast pulsed laser providing pulses with a duration  $\leq 1$  ps and sufficiently high power, but most importantly this laser should have a compact size to be flexibly transportable. Only recently such miniaturized mode-locked lasers based on semiconductor strip devices reliably operational with parameters that are attractive for PU experiments were designed [16-18]. Therefore, the task to establish PU pump-probe experiments exploiting these compact lasers can be tackled.

In the present paper we describe pump-probe PU experiments with mode-locked semiconductor strip lasers. As specimen for the PU studies we use an Al metal film, which is widely used as thermoelastic transducer in PU experiments [19], with a thickness of 112 nm. The measured pump-probe signals have similar signal to noise ratios as the signals obtained with a conventional PU setup based on commercial mode-locked titanium-sapphire laser. Finally, we discuss various possibilities for the development of a single chip based PU device on the basis of ASOPS technology [20] which does not require a bulky delay line in PU pump-probe experiments.

## 2. Mode-Locked Laser Device

In the experiments we used a laser fabricated by a MOCVD-grown AlGaAs/GaAs epilayer structure with an InGaAs-based active quantum-well (QW) region consisting of two 4.4 nm-thick

69 In<sub>0.18</sub>Ga<sub>0.82</sub>As QWs separated by a 9 nm-thick Al<sub>0.2</sub>Ga<sub>0.8</sub>As barrier. The parameters of the layers and the  
70 layer sequence are presented in Table 1. The active region, designed to emit at a wavelength of around 930  
71 nm, is sandwiched between two 120 nm graded-index AlGaAs layers and two Al<sub>0.32</sub>Ga<sub>0.68</sub>As claddings to  
72 provide electron and optical confinement. The lower AlGaAs cladding contains a graded far-field reduction  
73 layer that enlarges the mode size in the vertical direction, thus reducing both the vertical beam divergence  
74 and the optical power density [16].

75

76 **Table 1.** Epitaxial layer structure of the AlGaAs-based wafer.

Layer Type	Materials	THKNS μm	Dopant cm <sup>-3</sup>
Top Cladding			Zinc
CAP layer	GaAs	0.1	10 <sup>19</sup> ÷10 <sup>20</sup>
Matching	Al <sub>0.05</sub> Ga <sub>0.95</sub> As	0.12	10 <sup>18</sup> ÷5*10 <sup>18</sup>
p-cladding	Al <sub>0.32</sub> Ga <sub>0.68</sub> As	1.7	10 <sup>18</sup>
p-cladding	Al <sub>0.32</sub> Ga <sub>0.68</sub> As	0.2	5*10 <sup>17</sup> ÷10 <sup>18</sup>
Active			none
Graded Index	Al <sub>0.2</sub> Ga <sub>0.8</sub> As- Al <sub>0.32</sub> Ga <sub>0.68</sub> As	0.12	-
QW	In <sub>0.12</sub> Ga <sub>0.88</sub> As	0.0044	-
Barrier	Al <sub>0.2</sub> Ga <sub>0.8</sub> As	0.009	-
QW	In <sub>0.12</sub> Ga <sub>0.88</sub> As	0.0044	-
Graded Index	Al <sub>0.27</sub> Ga <sub>0.73</sub> As-Al <sub>0.2</sub> Ga <sub>0.8</sub> As	0.07	-
Bottom			Silicon
n-cladding	Al <sub>0.3</sub> Ga <sub>0.7</sub> As- Al <sub>0.27</sub> Ga <sub>0.73</sub> As	0.03	10 <sup>17</sup>
n-cladding	Al <sub>0.32</sub> Ga <sub>0.68</sub> As- Al <sub>0.27</sub> Ga <sub>0.73</sub> As	0.02	5*10 <sup>17</sup> ÷10 <sup>17</sup>
n-cladding	Al <sub>0.32</sub> Ga <sub>0.68</sub> As	0.75	5*10 <sup>17</sup>
F.F.R layer	Al <sub>0.29</sub> Ga <sub>0.71</sub> As- Al <sub>0.32</sub> Ga <sub>0.68</sub> As	0.35	5*10 <sup>17</sup>
F.F.R layer	Al <sub>0.32</sub> Ga <sub>0.68</sub> As- Al <sub>0.29</sub> Ga <sub>0.71</sub> As	0.35	5*10 <sup>17</sup>
n-cladding	Al <sub>0.32</sub> Ga <sub>0.68</sub> As	1.6	7*10 <sup>17</sup>
Matching	Al <sub>0.05</sub> Ga <sub>0.95</sub> As- Al <sub>0.32</sub> Ga <sub>0.68</sub> As	0.2	10 <sup>18</sup> ÷7*10 <sup>17</sup>
Substrate	GaAs	645	Silicon

77

78 The cross section of the laser is shown in Fig.1(a). The optical waveguide is fabricated by optical  
79 lithography and reactive ion etching with a SiCl<sub>4</sub> gas chemistry [21]. The waveguide has a width of 2.5 μm  
80 and an etching depth of approximately 2.1 μm to ensure single spatial mode operation. The total cavity  
81 length of 2.6 mm provides a cavity round trip time of 62 ps, corresponding to a repetition rate of 16 GHz  
82 under mode-locking conditions. The typical power-current voltage characteristics for such type of lasers is  
83 shown in Fig. 1(b). The passive mode-locking is achieved by introducing an intensity dependent loss  
84 element into the laser cavity, i.e., a saturable absorber. The absorber consists of an additional reversely  
85 biased section along the laser cavity [17]. Because of the saturation arising from the band filling effect,  
86 pulses as short as 1 ps can be generated under appropriate biasing conditions [18].

87 In the PU experiments we used a bar which consists of 20 lasers with identical design and similar  
88 characteristics. An optical image of a fragment of the bar is shown in Fig. 1 (c). The size of the chip is  
89 10x2.5 mm<sup>2</sup> while the size of the individual strip is 0.5x2.5 mm<sup>2</sup>. The laser emission spectra for different

90 absorber voltages measured at a bias current of 120 mA are shown in Fig.1 (d). It is seen that the emission  
 91 shifts to shorter wavelengths and the spectrum broadens with increasing voltage. In the PU experiments we  
 92 used 1.5 V on the absorber so that the laser emits at 928 nm.

93

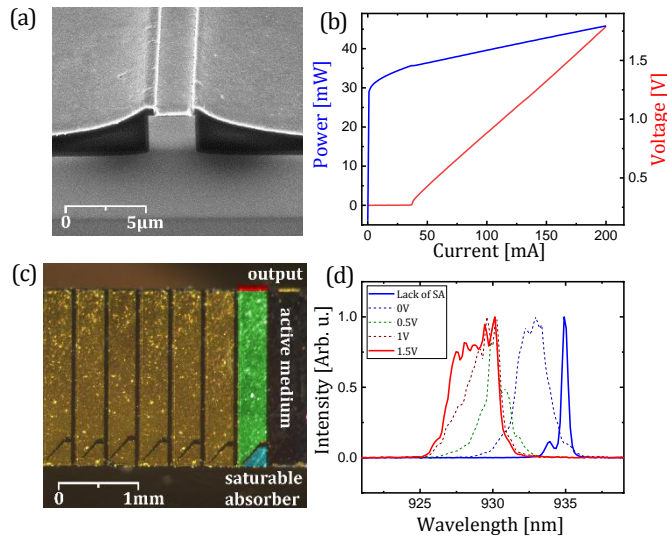


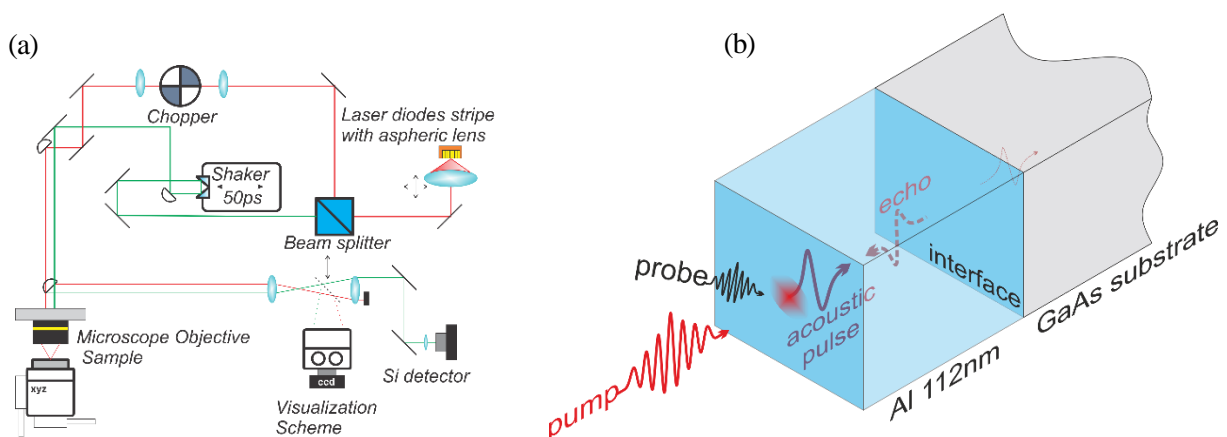
**Fig. 1.** Mode locked semiconductor laser: (a) cross section of the laser; (b) current voltage and output power characteristics of the laser with zero bias on the absorber; (c) optical image of the laser bars on the chip; (d) emission spectra of the laser for various biases applied to the absorber.

94

### 95 3. Experiment

96 The schematic of the PU pump probe setup is shown in Fig.2 (a). The laser beam is collimated by the  
 97 aspherical lens with focus distance of 3 mm. The beam is split into two paths for pump and probe. The  
 98 pump passes the chopper for 10 kHz frequency modulation and the probe is sent to the shaker in order to  
 99 achieve a variable time delay between the pulses in a range of up to 50 ps. Subsequently both beams go  
 100 through the x15 reflective microscope objective and are focused to a spot with a diameter of 5 μm on the  
 101 Al film as shown in Fig. 2(a). The average pump power used is 15 mW, which corresponds to ~4 μJ/cm<sup>2</sup>  
 102 excitation density on the Al film. The beams are reflected from the sample, the pump is blocked and the  
 103 probe beam is sent onto the silicon photodiode. A lock-in amplifier with the integration time of 3 ms is  
 104 used. For precise overlap on the sample, an optimized visualization scheme with a microscope set-up was  
 105 developed. The mirror controls allow one to adjust the pump and probe beam paths and to control precisely  
 106 the position of the two spots on the sample. The total area of the setup is 80x80 cm<sup>2</sup>.

107



108 **Fig. 2.** Experimental setup for picosecond ultrasonic experiments: (a) experimental schematic; (b) scheme  
 109 demonstrating the generation and detection of the echo strain pulse in the Al film.

110

111 Figure 3(a) shows the measured PU signal recorded with the semiconductor laser described above. The  
 112 pump pulse excites the Al film at  $t=0$ . The strong response observed in the time interval between  $t=0$  and  
 113 15 ps is typical for ultrafast pump-probe experiments [1,2,19] and is due to contributions from hot  
 114 electrons, rapid lattice heating and generated stress. The existence of several contributions makes it difficult  
 115 to extract the contribution from the generated stress and respective strain. The negative pulse with a  
 116 maximum at  $t=36$  ps corresponds to the first echo of the strain pulse reflected at the Al/GaAs interface as  
 117 shown in the inset of Fig. 2(b). Indeed, the arrival time of the maximum is expected at  $t_0=2d/s=35$  ps, where  
 118  $d=112$  nm is the nominal thickness of the Al film and  $s=6420$  m/s is the velocity of longitudinal sound in  
 119 Al. The slight difference of 1ps between the expected and measured values of the echo arrival time is due  
 120 to a slight difference between the actual and nominal thicknesses of the Al film. The reflection  $R$  of the  
 121 acoustic wave at the Al/GaAs interface depends on the acoustic impedances  $Z=\rho s$  of the materials, where  
 122  $\rho$  is the density:

$$123 \quad R = \frac{Z_{GaAs} - Z_{Al}}{Z_{GaAs} + Z_{Al}} \quad (1)$$

124 Substituting the values for  $Z$  into Eq. (1) we get  $R=0.2$  and the reflected strain pulse does not change the  
 125 phase at the Al/GaAs interface. If there was no contribution from the hot electrons at time around  $t=0$ , we  
 126 could expect a negative strain pulse with an amplitude 5 times larger than the amplitude of the echo signal.  
 127 At  $t=0$  the pump-probe signal is positive which means that the contribution from the hot electrons is several  
 128 times larger than the expected negative contribution from the thermo-elastic effect.

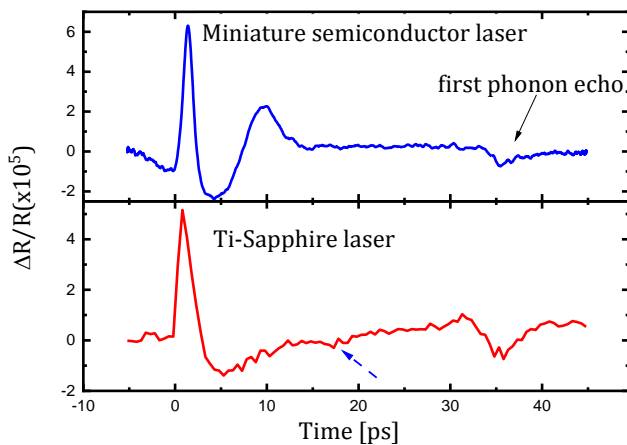


**Fig. 3.** Picosecond ultrasonic signals: (a) measured with the mode-locked semiconductor laser with repetition rate 16 GHz; (b) measured with 80 MHz commercial Ti-sapphire laser.

129

130 The PU signal in Fig. 3(a) measured with the miniaturized semiconductor laser has a shape similar  
 131 to the PU signals obtained in earlier experiments with Al films [19]. To be sure that our results obtained  
 132 with the semiconductor laser are basically identical to those obtained with a conventional femtosecond  
 133 laser, we performed PU experiments on the same Al film with a Ti-sapphire laser with 82 MHz repetition  
 134 rate at 900 nm wavelength and 150 fs pulse duration. However, the excitation energy density in the pump

135 pulse in this case is an order of magnitude higher, resulting in a stronger temperature rise of the Al film.  
136 The measured pump-probe trace is shown in Fig. 3(b). We see that the echo signal has a similar temporal  
137 shape and appears exactly at the same time as in the experiments with the miniaturized semiconductor laser.  
138 The measurement times in both experiments were the same, around 5 minutes, and the signal to noise ratios  
139 are almost the same. There is a difference in the temporal shapes around  $t=0$  which is likely due to the 200-  
140 fold difference in repetition rates and the incomplete recovery of the Al film to lattice temperature in the  
141 experiment with the semiconductor laser. In the experiments with Ti-Sapphire laser there is a barely visible  
142 signal at  $t=17-18$  ps marked by dashed arrow in Fig. 3. This feature, explained by the electron diffusion  
143 along the Al film [19], is not observed in experiments with semiconductor laser which likely due to much  
144 longer pulse duration and much higher repetitions rate relatively to Ti-Sapphire oscillator.

#### 145 **4. Discussion**

146 Our experiments show that miniaturized mode-locked semiconductor lasers are very well suitable  
147 for PU experiments. The typical property of these lasers is the high repetition rate which is given by the  
148 length of the laser cavity and typically is in the range of tens of GHz. The high repetition rate has the  
149 advantage of getting the required signal to noise ratio in a shorter time in comparison with conventional  
150 mode-locked lasers with repetition rates  $\sim 100$  MHz, using the same pump fluence in a single pulse.  
151 However, the disadvantage of the high-repetition rate is that the system potentially has no time to recover  
152 to the initial state. As we see in our experiments this does not have a significant effect on the echo signal,  
153 but could become important when studying PU signals that last longer than hundreds of picoseconds. The  
154 challenge of getting short laser pulses in miniaturized lasers with durations below a few ps may not be met  
155 with every laser and requires careful selection, but our experiments show that a temporal resolution of  $\Delta t \approx 1$   
156 ps can be achieved. The duration of the optical pulses which limits the temporal resolution of the PU  
157 experiments limits also the highest frequency of the detected acoustic wave. With durations of  $\sim 1$  ps for  
158 the pump and probe pulses, acoustic frequencies of several hundreds of GHz are achievable. PU  
159 experiments in this frequency range are high on demand in nondestructive material characterization and  
160 imaging of biological objects, including live cells.

161 The miniaturized mode-locked semiconductor lasers for PU experiments may have even higher  
162 average power than the one used so far: While this device relies on a standard two-segment ridge waveguide  
163 utilizing quantum well gain, great promise is held by implementing quantum dots as active gain material  
164 into the laser. Quantum dots offer several advantages for mode-locked operation of lasers such as a broad  
165 gain spectrum, a low linewidth enhancement factor, and ultrafast dynamics with low saturation energies. A  
166 second crucial step is the implementation of tapered mode-locked lasers, which consist of three segments:  
167 a saturable absorber to enable mode-locked operation, a ridge waveguide and a taper with an opening angle  
168 of a few degrees. In gain guided tapered lasers, the mode defined by the ridge waveguide is allowed to  
169 diffract into the taper without any lateral index discontinuities, under an angle (typically a few degrees)  
170 defined by the mode profile of the ridge. The width of the taper at the facet is an order of magnitude larger  
171 than that of a standard ridge waveguide, leading to a reduction of the power density and therefore the facet

172 load. In comparison to simple broad area lasers, which can provide only a moderate beam quality, tapered  
 173 lasers offer a very reasonable beam quality with beam parameter products ( $M^2$ ) below 2. This allows tight  
 174 focusing of the output beam from a tapered laser. In addition to the advantages for mode locked operation,  
 175 quantum dot active layers have also benefits for tapered lasers, in particular the small linewidth  
 176 enhancement factor, which reduces beam filamentation in the taper and therefore increases the beam quality  
 177 of the output.

178 In order to test this, we utilized an MBE-grown laser structure based on AlGaInAs quantum dot  
 179 laser material, emitting at  $\sim 920$  nm. The QDs were embedded in a 250 nm thick AlGaAs graded index  
 180 heterostructure (GRINSCH), and a symmetric AlGaAs cladding (see Table 2). The waveguide structures  
 181 were defined by electron-beam lithography and reactive ion etching, yielding devices with an overall  
 182 length of 2.250 mm and an absorber length ranging from 50 to 400  $\mu\text{m}$ . In order to observe the transition  
 183 from normal to mode-locked operation, the output of the laser was analyzed using a fast fiber-coupled  
 184 optical receiver and a microwave spectrum analyzer. A significant narrowing of the RF-spectra was  
 185 observed when reverse bias was applied to the absorber segment, indicating the onset of mode-locking.  
 186 The peak of the RF frequency (see Fig. 4) is located at 18.05 GHz, corresponding to a cavity round trip  
 187 time of 55.4 ps.

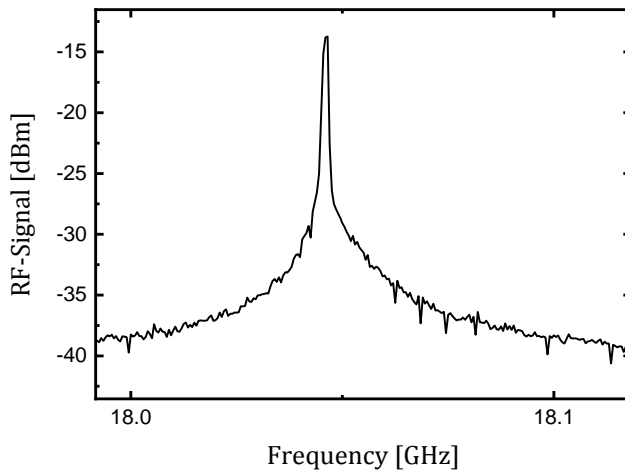


**Fig. 4.** Microwave spectrum of the mode-locked quantum dot laser.

188

189

190

**Table 2.** Epitaxial layer structure of the QD based wafer.

Layer Type	Materials	THKNS $\mu\text{m}$	Dopant
Top Cladding			Beryllium
CAP layer	GaAs	0.25	
p-cladding	$\text{Al}_{0.40}\text{Ga}_{0.60}\text{As}$	1.5	
Active Medium			none
GRINSH	GaAs/AlGaAs SSL, $\text{Al}_{0.18}\text{Ga}_{0.82}\text{As}$	0.25	-
Barrier	GaAs	0.003	-
SK QD 4.9ML	$\text{Al}_{0.15}\text{Ga}_{0.23}\text{In}_{0.62}\text{As}$	-	-
Barrier	GaAs	0.003	-

GRINSH	GaAs/AlGaAs SSL, Al <sub>0.18</sub> Ga <sub>0.82</sub> As	0.25	-
Bottom Cladding			Silicon
n-cladding	Al <sub>0.40</sub> Ga <sub>0.60</sub> As	1.5	
Substrate	GaAs	-	Silicon

191

192 Implementing a mode-locked miniaturized laser is the first step in creating a portable PU setup. Another  
 193 quite massive element in standard PU setups is the delay line. The best solution there will be using  
 194 Asynchronous Optical Sampling (ASOPS) [20], which requires two mode-locked semiconductor lasers.  
 195 For this the jitter of the pulses defined by the noise in the laser becomes extremely important. Nowadays  
 196 the jitter in monolithic semiconductor mode-locked lasers is below 100fs and by using external feedback  
 197 it may be as small as 23fs [22] which does not reduce the temporal resolution for 1 ps long laser pulses.

198 This will pave the way for realizing portable sub-THz acoustic equipment for in-situ picosecond  
 199 ultrasonic studies.

200 In conclusion, we have demonstrated picosecond ultrasonic setup on the basis of miniaturized  
 201 mode-locked semiconductor laser. The measurement of a picosecond acoustic echo in Al film shows that  
 202 the ultrasonic signal has the same shape and signal to noise ratio as in conventional setups with bulky mode-  
 203 locked lasers. The experiments show the prospective of designing and developing portable picosecond  
 204 ultrasonic setups integrated on a chip for utilization in medicine, biology and geology.

#### 205 **CRedit authorship contribution statement**

206 **Michal Kobecki, Alexey V. Scherbakov, Thomas Czerniuk:** Picosecond ultrasonic setup and  
 207 measurements, preparing manuscript. **Giuseppe Tandoi, Eugenio Di Gaetano, Marc Sorel:**  
 208 Fabrication of MOCVD lasers; editing manuscript. **Christian Schneider, Martin Kamp, Sven**  
 209 **Höfling:** Fabrication of MBE lasers; editing manuscript. **Andrey V. Akimov,** Conceptualization,  
 210 first draft of the manuscript. **Manfred Bayer:** Supervision, conceptualization, editing the  
 211 manuscript

#### 212 **Acknowledgement**

213 The work was supported by the Bundesministerium für Bildung und Forschung through the project “Nano-  
 214 Akusto-Mechanik mit integriertem Laser (NAMIL)” (FKZ 13N14071) and the Deutsche  
 215 Forschungsgemeinschaft in the frame of TRR 142 (project A6). We are thankful to Dirk Schemionek for  
 216 depositing the Al films for the picosecond acoustic experiments.

217

#### 218 **References**

- 219 1. C. Thomsen, H.T. Grahn, H.J. Maris and J. Tauc, “Surface generation and detection of phonons  
 220 by picosecond light pulses,” Phys. Rev. B 34, 4129–4138 (1986).  
 221 2. O. Matsuda, M.C. Larciprete, R. Li Voti and O.B. Wright, “Fundamentals of picosecond laser  
 222 ultrasonics,” Ultrasonics 56, 3-20 (2015).

- 223 3. K.H. Lin, C.M. Lai, C.C. Pan, J.I. Chyi, J.W. Shi, S.Z. Sun, C.F. Chang and C.K. Sun, "Spatial  
224 Manipulation of Nanoacoustic Waves with Nanoscale Spot Sizes," *Nat. Nanotechnol.* 2, 704-708  
225 (2007).
- 226 4. D. M. Moss, A.V. Akimov, B.A. Glavin, M. Henini, and A.J. Kent, "Ultrafast Strain-Induced  
227 Current in a GaAs Schottky Diode", *Phys. Rev. Lett.* 106, 066602 (2011).
- 228 5. C. Brüggemann, A.V. Akimov, A.V. Scherbakov, M. Bombeck, C. Schneider, S. Hofling, A.  
229 Forchel, D. R. Yakovlev, and M. Bayer, "Laser mode feeding by shaking quantum dots in a  
230 planar microcavity," *Nat. Photon.* 6, 30-34 (2012).
- 231 6. A.V. Scherbakov, A.S. Salasyuk, A.V. Akimov, X. Liu, M. Bombeck, C. Brüggemann, D.R.  
232 Yakovlev, V.F. Sapega, J.K. Furdyna, and M. Bayer, "Coherent Magnetization Precession in  
233 Ferromagnetic (Ga,Mn)As Induced by Picosecond Acoustic Pulses," *Phys. Rev. Lett.* 105,  
234 117204 (2010).
- 235 7. A.Vertikov, M. Kuball, A.V. Nurmikko and H.J. Maris, "Time-Resolved Pump-Probe  
236 Experiments with Subwavelength Lateral Resolution," *Appl. Phys. Lett.* 69, 2465-2767 (1996).
- 237 8. T. Dehoux, K. Ishikawa, P.H. Otsuka, M. Tomoda, O. Matsuda, M. Fujiwara, S. Takeuchi, I.A.  
238 Veres, V.E. Gusev and O.B. Wright, "Optical Tracking of Picosecond Coherent Phonon Pulse  
239 Focusing Inside a sub-Micron Object," *Light: Sci. Appl.* 5, e16082 (2016).
- 240 9. H. Ogi, T. Kawamoto, N. Nakamura, M. Hirao, and M. Nishiyama, "Ultrathin-film oscillator  
241 biosensors excited by ultrafast light pulses," *Biosens Bioelectron* 26, 1273 (2010).
- 242 10. T. Dehoux and B. Audoin, "Non-invasive optoacoustic probing of the density and stiffness of  
243 single biological cells," *Appl. Phys. Lett.* 12, 124702 (2012).
- 244 11. T. Dehoux, M. Abi Ghanem, O.F. Zouani, J.M. Rampnoux, Y. Guillet, S. Dilhaire, M.C. Durrieu,  
245 and B. Audoin, "All-optical broadband ultrasonography of single cells," *Sci. Rep.* 5, 8650 (2015).
- 246 12. C.C. Shen, M.Y. Weng, J.K. Sheu, Y. T. Yao and C. K. Sun, "In Situ Monitoring of Chemical  
247 Reactions at a Solid–Water Interface by Femtosecond Acoustics," *J. Phys. Chem. Lett.* 8, 5430-  
248 5437 (2017).
- 249 13. Y. Guillet, B. Audoin, M. Ferrié and S. Ravaine, "All-Optical Ultrafast Spectroscopy of a Single  
250 Nanoparticle-Substrate Contact," *Phys. Rev. B* 86, 035456 (2012).
- 251 14. J.D.G. Greener, A.V. Akimov, V.E. Gusev, Z.R. Kudrynskyi, P.H. Beton, Z.D. Kovalyuk, T.  
252 Taniguchi, K. Watanabe, A.J. Kent and A. Patané, "Coherent Acoustic Phonons in van der Waals  
253 Nanolayers and Heterostructures," *Phys. Rev. B* 98, 075408 (2018).
- 254 15. C. Mechri, P. Ruello, J.M. Breteau, M.R. Baklanov, P. Verdonck and V. Gusev, "Depth profiling  
255 of elastic inhomogeneities in transparent nanoporous low-k materials by picosecond ultrasonic  
256 interferometry," *Appl. Phys. Lett.* 95, 091907 (2009).
- 257 16. L. Hou, M. Haji, J. H. Marsh and A. C. Bryce "10 GHz AlGaInAs/InP 1.55um passively mode-  
258 locked laser with low divergence angle and timing jitter," *Opt. Express* 19, B75-B80 (2011).
- 259 17. M.J. Lederer, V. Kolev, B. Luther-Davies, H.H. Tan and C. Jagadish, "Ion-implanted InGaAs  
260 single quantum well semiconductor saturable absorber mirrors for passive mode-locking,"  
261 *Journal of Physics D: Applied Physics* 34, 2455 (2001).
- 262 18. F.X. Kärtner, I.D. Jung and U. Keller "Soliton Mode-Locking with Saturable Absorber," *IEEE*  
263 *Journal of selected topics in quantum electronics* 2, 540 - 556 (1996).
- 264 19. G. Tas and H.J. Maris, "Electron diffusion in metals studied by picosecond ultrasonics," *Phys.*  
265 *Rev. B* 49, 15046 (1994).
- 266 20. A. Bartels, F. Hudert, C. Janke, T. Dekorsy and K. Köhler, "Femtosecond time-resolved optical  
267 pump-probe spectroscopy at kilohertz-scan-rates over nanosecond-time-delays without  
268 mechanical delay line," *Appl. Phys. Lett.* 88, 041117 (2006).
- 269 21. S.J. Pearton, U.K. Chakrabarti, W.S. Hobson and A.P. Kinsella, "Reactive Ion Etching of GaAs,  
270 AlGaAs, GaSb in Cl<sub>2</sub> and SiCl<sub>4</sub>," *J. Vac. Sci. Technol. B* 8, 607-617 (1990).
- 271 22. D. Arsenijevic, M. Kleinert, and D. Bimberg, "Phase noise and jitter reduction by optical  
272 feedback on passively mode-locked quantum-dot lasers," *Appl. Phys. Lett.* 103, 231101 (2013).

Declaration of Competing Interest

The authors declared that there is no conflict of interest.